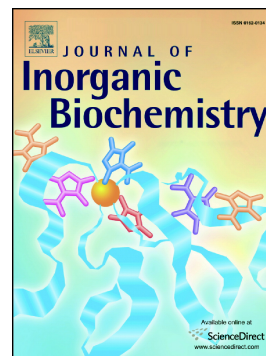


Journal Pre-proof

Picolinate-appended tacn complexes for bimodal imaging: Radiolabeling, relaxivity, photophysical and electrochemical studies

Amaury Guillou, Margaux Galland, Amandine Roux, Balázs Váradi, Réka Anna Gogolák, Patricia Le Saëc, Alain Faivre-Chauvet, Maryline Beyler, Christophe Bucher, Gyula Tircsó, Véronique Patinec, Olivier Maury, Raphaël Tripier



PII: S0162-0134(19)30597-5

DOI: <https://doi.org/10.1016/j.jinorgbio.2019.110978>

Reference: JIB 110978

To appear in: *Journal of Inorganic Biochemistry*

Received date: 16 September 2019

Revised date: 11 December 2019

Accepted date: 24 December 2019

Please cite this article as: A. Guillou, M. Galland, A. Roux, et al., Picolinate-appended tacn complexes for bimodal imaging: Radiolabeling, relaxivity, photophysical and electrochemical studies, *Journal of Inorganic Biochemistry* (2018), <https://doi.org/10.1016/j.jinorgbio.2019.110978>

This is a PDF file of an article that has undergone enhancements after acceptance, such as the addition of a cover page and metadata, and formatting for readability, but it is not yet the definitive version of record. This version will undergo additional copyediting, typesetting and review before it is published in its final form, but we are providing this version to give early visibility of the article. Please note that, during the production process, errors may be discovered which could affect the content, and all legal disclaimers that apply to the journal pertain.

© 2018 Published by Elsevier.

Picolinate-Appended Tacn Complexes for Bimodal Imaging: radiolabeling, relaxivity, photophysical and electrochemical studies

Amaury Guillou,^a Margaux Galland,^b Amandine Roux,^b Balázs Váradi,^c Réka Anna Gogolák,^c

Patricia Le Saëc,^d Alain Faivre-Chauvet,^d Maryline Beyler,^a Christophe Bucher,^b Gyula

Tircsó,^c Véronique Patinec,^{*a} Olivier Maury^{*b}, and Raphaël Tripier^{*a}

^a *Univ Brest, UMR-CNRS 6521 CEMCA, 6 avenue Victor le Gorgeu, 29200 Brest, France.
raphael.tripier@univ-brest.fr*

^b *Univ Lyon, ENS Lyon, CNRS, Université Lyon 1, Laboratoire de Chimie, UMR 5182, 46 allée d'Italie, 69364
Lyon, France. Olivier.Maury@ens-lyon.fr*

^c *Department of Physical Chemistry, Faculty of Science and Technology, University of Debrecen, Egyetem tér 1, H-
4032 Debrecen, Hungary.*

^d *Université de Nantes, Centre de Recherche en Cancérologie et Immunologie Nantes Angers (CRCINA), Unité
INSERM 1232 – CNRS 6299, 8 quai Moncousu, BP 70721, 44007 Nantes Cedex, France.*

ABSTRACT

Based on our previous works involving two 1,4,7-triazacyclononane (tacn)-based ligands **Hno2py1pa** (1-Picolinic acid-4,7-bis(pyridin-2-ylmethyl)-1,4,7-triazacyclononane) and **Hno1pa** (1-Picolinic acid-1,4,7-triazacyclononane), we report here the synthesis of analogues bearing picolinate-based π -conjugated ILCT (Intra-Ligand Charge Transfer) transition antenna (**HL1**, **HL2**), using regiospecific *N*-functionalization of the tacn skeleton and their related transition metal complexes (*e.g.* Cu^{2+} , Zn^{2+} and Mn^{2+}). Coordination properties as well as their photophysical and electrochemical properties were investigated in order to quantify the impact of such antenna on the luminescent or relaxometric properties of the complexes. The spectroscopic properties of the targeted ligands and metal complexes have been studied using UV-Vis absorption and fluorescence spectroscopies. While the zinc complex formed with **HL1** possesses a moderate quantum yield of 5%, complexation of Cu^{2+} led to an extinction of the luminescence putatively attributed to a photo-induced electron transfer, as supported by spectroscopic and electrochemical evidences. The $[\text{Mn}(\text{L2})]^+$ complex is characterized by a fluorescence quantum yield close to 8% in CH_2Cl_2 . The potential interest of such systems as bimodal probes has been assessed from radiolabeling experiments conducted on **HL1** and $^{64}\text{Cu}^{2+}$ as well as confocal microscopy analyses and from relaxometric studies carried out on the cationic $[\text{Mn}(\text{L2})]^+$ complex. These results showed that **HL1** can be used for radiolabeling, with a radiochemical conversion of 40% in 15 minutes at 100°C . Finally, the relaxivity values obtained for $[\text{Mn}(\text{L2})]^+$, $r_{1p} = 4.80 \text{ mM}^{-1}\cdot\text{s}^{-1}$ and $r_{2p} = 8.72 \text{ mM}^{-1}\cdot\text{s}^{-1}$, make the Mn(II) complex an ideal candidate as a probe for Magnetic Resonance Imaging.

1. Introduction

Current molecular imaging and therapy techniques used in medicine, such as Positron Emission Tomography (PET), Optical Imaging (OI), Magnetic Resonance Imaging (MRI) or RadioImmunoTherapy (RIT) exploit the intrinsic radioactive, optical or magnetic properties of transition metals (*i.e.* $^{52}\text{Mn}^{2+}$, $^{64}\text{Cu}^{2+}$, $^{68}\text{Ga}^{3+}$, $^{89}\text{Zr}^{4+}$, etc...), lanthanides (*i.e.* Gd^{3+} , Eu^{3+} , Yb^{3+}) or organic fluorophores to produce visualization techniques for diagnosis or direct therapy of disease, especially for cancer [1,2]. Each technique presents its own advantages and drawbacks. For example, the main limitations of fluorescence imaging is the lack of depth penetration of the incident or emitted light while PET presents a low resolution and MRI lacks sensitivity. PET, MRI and OI thus stand as fully complementary techniques that could be advantageously combined to achieve more accurate diagnosis [3]. Such combinations can be realized through the development of multimodal probes involving coordination complexes as key functional /building elements [4,5]. Beyond multimodality, the selected metal-containing probes to be used in biological media must comply with essential stability and solubility standards.

Given the growing importance of bimodal imaging, the design of functional polyazamacrocyclic ligands has recently become a very active field of research [6-9]. Despite being the smallest saturated polyazamacrocycle, the tacn (1,4,7-triazacyclononane) macrocycle has proved to be capable, when appropriately *N*-functionalized, to stabilize a wide range of metal ions starting from the smallest transition metal ions to the largest lanthanides [10-12]. In line with this strategy, some of us have recently developed a series of *N*-functionalized tacn chelators bearing picolinate pendants (**Hno2py1pa** and **Hno1pa**, Figure 1) used, after complexation with Cu^{2+} or Mn^{2+} , as PET [13] or MR [14] imaging agents. Indeed, Cu^{2+} is widely used in nuclear medicine due to the availability of ^{64}Cu isotope (β^+ emitter, $t_{1/2} = 12.7$ h) suitable for PET imaging. On the other hand, high spin ($S = 5/2$) Mn^{2+} complexes have been considered as viable alternatives to the gadolinium (III) complexes currently used

in MRI [15]. In order to further implement an optical imaging modality to these scaffolds, we envisaged to functionalize the picolinate pendant arm by suitable electron rich π -conjugated chromophore selected for their ability to act as effective antennas for lanthanide sensitization under one or two-photon excitation (Figure 1) [16,17].

[Figure 1 here]

In this paper, we present the synthesis and detailed characterizations of two original ligands **HL1**, **HL2** and of their corresponding metal complexes with Cu^{2+} , Zn^{2+} and Mn^{2+} (including radiolabeling with $^{64}\text{Cu}^{2+}$). Their photophysical, electrochemical and relaxivity properties have been thoroughly investigated to evaluate their potential as bimodal probes.

2. Experimental

Reagents were purchased from ACROS Organics and from Aldrich Chemical Co. Reagents used in radiolabeling process are « trace select » grade. 1,4,7-triazacyclononane (tacn) was purchased from CheMatech (Dijon, France). Acetonitrile, THF and water solvents were distilled before use. HRMAs analyses were performed at ICOA, Orléans, France. NMR spectra were recorded at the “Services communs” of the University of Brest. ^1H and ^{13}C NMR spectra were recorded with Bruker Avance 500 (500 MHz), Bruker Avance 400 (400 MHz), or Bruker AMX-3 300 (300 MHz) spectrometers. Dialysis purification were performed using Float-A-Lyzer[®] dialysis device (MWCO = 100-500 D). Briefly, the membrane was activated using a 20% iPrOH in H_2O ($>18.2 \text{ M}\Omega\cdot\text{cm}$ at 25°C) and then washed 3 times with water. The sample was loaded and the device was put in 500 mL of H_2O and stirred for 4 h, the process was repeated twice. The synthesis of the functionalized picolinate pendant **a** (Scheme 1), featuring dialkylamino phenylethynyl conjugated skeleton, was achieved through a

modification of a previously published procedure (see in Supporting Informations, Text S1 and Figures S1-S6) [18,19]. This key fragment was then further “decorated” by oligo-ethylene glycol substituents to improve the solubility of the resulting complexes in biological media. All the spectra corresponding to **HL1** and **HL2** characterization are in Supporting Informations, Figures S7-S15.

2.1. Synthesis of the ligands

Ligand HL1. A solution of the mesylated antenna **a** (Methyl 4-[4-ethynyl-*N,N*-bis(3,6,9-trioxodecyl)aniline]-6-[(methylsulfonyloxy)methyl]-2-picolinate) (600 mg, 0.92 mmol) (Scheme 1) in acetonitrile (30 mL) was added dropwise to a solution of **no2py** (4,7-bis(pyridin-2-ylmethyl)-1,4,7-triazacyclononane) (288 mg, 0.92 mmol). The solution was stirred at room temperature for 4 days, filtered and the solvent evaporated under reduced pressure. The crude product was purified by chromatography on neutral Alumina (CHCl₃ to CHCl₃/MeOH 85/15). The purified compound was then dialyzed to yield 1-{4-[4-ethynyl-*N,N*-bis(3,6,9-trioxodecyl)aniline]-2-methoxycarbonyl}pyridin-2-ylmethyl-4,7-bis(pyridin-2-ylmethyl)-1,4,7-triazacyclononane (compound **1**) as a yellow oil (439 mg, 55 %).

¹H NMR (CDCl₃, 300 MHz, 298 K) δ (ppm) 2.85-2.90 (m, 11H, CH₂ tacn) 3.34 (s, 6H, CH₃) 3.51-3.61 (m, 24H, CH₂) 3.83 (s, 4H, CH₂) 3.90 (s, 2H, CH₂) 3.95 (s, 3H, CH₃) 6.63 (d, 2H, ³J= 9 Hz) 7.07 (t, 2H, ³J= 5 Hz) 7.34 (d, 2H, ³J= 9 Hz) 7.49 (d, 2H, ³J= 8 Hz) 7.59 (t, 2H, ³J= 3 Hz) 7.78 (s, 1H) 8.00 (s, 1H) 8.46 (d, 2H, ³J= 4 Hz). ¹³C NMR (CDCl₃, 75 MHz, 298 K) δ (ppm) 50.6 (CH₂ βN) 52.7 (CH₃) 55.3, 55.6 (CH₂ tacn) 58.8 (CH₃) 63.9 (CH₂) 64.4 (CH₂) 68.1, 70.3, 70.4, 70.5, 71.7 (CH₂) 85.0 (Cqt) 96.7 (Cqt) 107.8 (Cqt) 111.2 (CH) 121.7 (CH) 123.1 (CH) 125.0 (CH) 127.1 (CH) 133.2 (CH) 133.6 (Cqt) 136.1 (CH) 147.0 (Cqt) 148.4 (Cqt) 148.6 (Cqt) 165.4 (C=O). **ESI-HRMS** m/z calcd. for [C₄₈H₆₆N₇O₈+H]⁺ 868.4967, found 868.4962.

The intermediate **1** (100 mg, 0.11 mmol) was then dissolved in THF (4 mL) and 1M KOH_(aq) (2 mL) was added. The mixture was stirred at 55°C for 3 h and concentrated under reduced pressure. The crude was dissolved in H₂O (3 mL) and the pH was adjusted to 3 with HCl 1M. The product was dialyzed yielding 1-{2-carboxy-4-[4-ethynyl-*N,N*-bis(3,6,9-trioxodecyl)aniline]}pyridyn-2-ylmethyl-4,7-bis(pyridin-2-ylmethyl)-1,4,7-triazacyclononane **HL1** as a yellow oil (97 mg, 99%).

¹H NMR (D₂O, 500 MHz, 298 K) δ (ppm) 2.73 – 2.95 (m, 8H, CH₂ tacn) 3.26 – 3.30 (m, 9H, CH₃ PEG) 3.45 – 3.51 (m, 28H, CH₂ tacn + CH₂ PEG) 3.79 (s, 2H) 3.88 (s, 2H) 6.61 (m, 2H) 7.15 – 7.17 (m, 3H) 7.19 – 7.25 (m, 2H) 7.35 (m, 2H) 7.73 (m, 1H) 7.80 (m, 1H) 8.41 (s, 1H). **¹³C NMR** (D₂O, 126 MHz, 298 K) δ (ppm) 51.5, 51.9 (CH₂ tacn) 52.8 (CH₂ β N) 53.8 (CH₂ tacn) 60.9 (CH₃) 62.9 (CH₂) 64.5 (CH₂) 65.3 (CH₂) 70.6, 71.2, 72.3, 72.5, 72.8, 73.9, 74.9 (CH₂) 88.8 (Cqt) 99.9 (Cqt) 110.1 (Cqt) 114.8 (CH) 125.7 (CH) 126.6 (CH) 127.3 (CH) 128.9 (CH) 136.1 (Cqt) 136.4 (CH) 140.8 (CH) 151.7 (CH) 156.5 (Cqt) 156.8 (Cqt) 160.7 (Cqt) 173.8 (C=O). **ESI-HRMS** m/z calcd. for [C₄₇H₆₅N₇O₈+H]²⁺ 427.7441, found 427.7446.

Ligand HL2. To a solution of 1,4,7-triazacyclononane (450 mg, 3.48 mmol) in distilled ethanol (70 mL) containing molecular sieves was added benzaldehyde (369 mg, 3.48 mmol). The reaction mixture was stirred for 4 h, then filtered through a pad of Celite[®] and the solvent was removed under reduced pressure, yielding 10-phenyl-1,4,7-triazabicyclo[5.2.1]decane **2** as a white solid (750 mg, 95%).

¹H NMR (CDCl₃, 300 MHz, 298 K) δ (ppm) 2.89-2.93 (4H, m, CH₂ tacn); 2.99-3.03 (2H, m, CH₂ tacn); 3.07-3.17 (4H, m, CH₂ tacn); 3.32-3.39 (2H, m, CH₂ tacn); 5.66 (1H, s, CH aminal); 7.18 (1H, t, ³J= 7.3 Hz, CH_{Ar}); 7.29 (2H, t, ³J= 7.3 Hz, CH_{Ar}); 7.50 (2H, d, ³J= 7.3 Hz, CH_{Ar}). **¹³C NMR** (CDCl₃, 75 MHz, 298 K) δ (ppm) 49.3, 49.6, 58.8 (CH₂ tacn) 88.3 (CH) 126.6, 126.7, 128.2 (CH_{Ar}) 145.8 (Cqt).

Compound **2** (400 mg, 1.84 mmol) was dissolved in acetonitrile (100 mL) and K_2CO_3 (508 mg, 3.68 mmol) was added before addition of a solution containing **a** (1.2 g, 1.84 mmol) (Scheme 1) in acetonitrile (50 mL) over a period of 30 min. The reaction was stirred at room temperature for 2 days. Filtration through Celite[®] and evaporation of the solvent gave a crude yellow oil that was purified by column chromatography (Al_2O_3 , CH_2Cl_2 100% to CH_2Cl_2 / MeOH / isopropylamine 90: 7: 3) to yield deprotected compound 1-{4-[4-ethynyl-*N,N*-bis(3,6,9-trioxodecyl)aniline]-2-methoxycarbonyl}pyridin-2-ylmethyl-1,4,7-triazacyclononane **3** as a yellow oil (781 mg, 62 % over two steps).

¹H NMR ($CDCl_3$, 300 MHz, 298 K) δ (ppm) 2.74 (s, 8H, CH_2 tacn) 2.85 (s, 4H, CH_2 tacn) 3.00 (s, 2H, NH) 3.35 (s, 6H, CH_3) 3.51 – 3.62 (m, 24H, CH_2) 3.96 (s, 2H, CH_2) 3.98 (s, 3H, CH_3) 6.94 - 6.98 (d, $^3J = 8.9$ Hz, 2H, CH) 7.35 - 7.38 (s, $^3J = 8.8$ Hz, 2H, CH) 7.61 (s, 1H, CH) 8.01 (s, 1H, CH). ¹³C NMR ($CDCl_3$, 75 MHz, 298 K) δ (ppm) 46.7, 47.1, 50.9 (CH_2 tacn) 53.1 (CH_3) 53.2 (CH_2) 59.1 (CH_3) 61.7 (CH_2) 68.4, 70.7, 70.7, 70.8, 72.0 (CH_2 PEG) 85.1 (Cqt) 97.4 (Cqt) 108.1 (Cqt) 111.5 (CH) 125.5 (CH) 127.1 (CH) 133.6 (CH) 134.2 (Cqt) 147.5 (Cqt) 148.7 (Cqt) 161.0 (Cqt) 165.6 (C=O). ESI-HRMS m/z calcd. for $[C_{36}H_{56}N_5O_8]^+$ 686.4123, found 686.4124.

Finally, compound **3** (200 mg, 0.29 mmol) was dissolved in THF and 1M KOH (2 mL) was added. The mixture was stirred at 50°C for 3 h and then concentrated under reduced pressure. The crude product was purified by semi-preparative HPLC yielding the final ligand 1-{2-carboxy-4-[4-ethynyl-*N,N*-bis(3,6,9-trioxodecyl)aniline]}pyridin-2-ylmethyl-1,4,7-triazacyclononane **HL2** as a yellow oil (188 mg, 97%).

¹H NMR (D_2O , 300 MHz, 298 K) δ (ppm) 3.12 (m, 4H), 3.25-3.34 (m, 12H) 3.47-3.58 (m, 19H) 3.68-3.78 (m, 13H) 4.18 (s, 2H, CH_2 α N) 7.07-7.10 (d, $^3J = 9$ Hz, 2H) 7.48 (s, 1H) 7.97-8.00 (d, $^3J = 9$ Hz, 3H). ¹³C NMR (D_2O , 75 MHz, 298 K) δ (ppm) 46.1, 47.5, 51.6, 54.7, 60.0 (CH_2) 60.8 (CH) 69.7, 72.3, 72.7, 73.8 (CH_2 PEG) 117.3 (CH_{Ar}) 121.1 (Cqt) 129.0 (CH_{Ar})

129.3 (Cqt) 131.0 (CH_{Ar}) 134.1 (CH_{Ar}) 149.4, 151.5, 152.8, 162.2 (Cqt) 198.0 (C=O). **ESI-HRMS** m/z calcd. for [C₃₅H₅₄N₅O₈]⁺ 672.3966, found 672.3966.

2.2. Synthesis and characterisation of the complexes

General procedure for the synthesis of the [M^{II}L1] complexes (M^{II} = Cu²⁺/Zn²⁺)

Ligand **HL1** (10 mg, 0.01 mmol) was dissolved in ultra-pure deionized H₂O (5 mL), and the pH of the solution was adjusted to pH = 5. Then M(ClO₄)₂·6H₂O (0.01 mmol) was added and the pH was adjusted to 6.6. The mixture was stirred for 24 h at 60°C. The resulting crudes were purified by semi-preparative HPLC (see in Supporting Informations, Figures S16-S19) and lyophilized.

[Cu(**L1**)](ClO₄): yellow oil (10 mg, 94%). **ESI-HRMS** m/z calcd. for [C₄₇H₆₃N₇O₈Cu]²⁺ 458.2011, found 458.2015.

[Zn(**L1**)](ClO₄): yellow oil (9.8 mg, 90%). **ESI-HRMS** m/z calcd. for [C₄₇H₆₃N₇O₈Zn]²⁺ 459.7014, found 459.7009.

Synthesis of [MnL2]⁺ complex

A procedure similar to the one used for **HL1** complexes has been followed starting from **HL2** (0.01 mmol) and MnCl₂·4H₂O (0.01 mmol) to lead to [Mn(**L2**)](Cl) complex as a yellow oil (6.8 mg, 60%). Our attempts to characterize the Mn²⁺ complex via HR-MS unfortunately failed although the HPLC obtained confirmed its formation /existence and purity (see in Supporting Informations, Figure S20). Additionally, as explained below, the pH-potentiometric and relaxation experiments also confirmed its formation.

2.3. Radiolabeling with ⁶⁴Cu

⁶⁴CuCl₂ in 0.1 M HCl was added in a molar ratio 1:1 equivalent into 0.1 M acetate pH = 5.5

buffered ligand solution. The reaction mixture was incubated at 100°C for 15 min. Then the radiolabeling was quenched through addition of a calculated volume of 1 mM EDTA pH = 5 to obtain a ratio EDTA-to-ligand of 10 and the mixture was stirred at room temperature for 10 min. 2 μ L of this solution was taken out and deposited on a silica gel plate (Silica Gel 60F254, Merck). The thin layer chromatography was developed for 7 cm using a mixture of ammonium chloride 20% in water:methanol (1:1/v:v). The plate was then removed from the solvent and exposed for 5 min on a storage phosphor plate, and this was revealed using a radiometric phosphor imager Cyclone® Plus (PerkinElmer) and analyzed with the Optiquant® software to obtain a radiochromatogram.

2.4. r_{1p} and r_{2p} relaxivities of the Mn^{2+} complex

Relaxation times of water protons were measured at 60 MHz with a Bruker Minispec MQ-60 NMR Analyzer. The temperature of the sample holder was set ($25.0 \pm 0.2^\circ C$) and controlled with the use of a circulating water bath. The longitudinal relaxation times (T_1) were measured by using the inversion recovery method ($180^\circ - t - 90^\circ$) by averaging 5-6 identical data points obtained at 14 different t values. The transverse relaxation times (T_2) were measured by using the Carr-Purcell-Meiboom-Gill sequence (CPMG) sequence again by averaging 5-6 identical data points.

The r_{1p} and r_{2p} relaxivities of the complex were determined by using batch samples which were prepared under nitrogen atmosphere having the ligand present at a 1.5 mM concentration (the pH in these samples was kept constant at pH = 8.12 with the use of HEPES buffer ($I = 0.15$ M NaCl, $25^\circ C$)). Various amounts of $MnCl_2$ were added to these solutions and the relaxation times of the solutions were measured. By relying on the species distribution curves under these conditions, only one Mn^{2+} ion containing species is present in solution which is the $[Mn(L2)]$ complex. The curve obtained by plotting $1/T_{1,2p}$ as a function of Mn^{2+}

concentration for the samples with $[L] > [Mn^{2+}]$ gives a straight line, with a slope that is equal to r_{1p} and r_{2p} relaxivities respectively. To confirm the complex formation and its pH range, a sample containing 1 mM of the ligand and Mn^{2+} ion ($V_{tot} = 10$ mL) was titrated with NaOH under N_2 protected atmosphere and the $1/T_{1,2p}$ data was collected in the pH range of 3.0-11.0. The given data co-plotted with the species distribution curve calculated based on the stability constants determined by pH-potentiometric method were in excellent agreement.

2.5. Potentiometric measurements of the Mn^{2+} complex

The protonation constants of the ligands were determined by pH-potentiometric titrations carried out with a Metrohm 888 Titrando titration workstation using a Metrohm 6.0233.100 combined electrode. The titrated solutions (6.00 mL) were thermostated at 25°C and the ionic strength in the samples was set to 0.15 M NaCl. The samples were stirred and kept under inert gas atmosphere (N_2) to avoid the effect of CO_2 . For the pH-calibration of the electrode standard buffers (KH-phthalate (pH=4.005) and borax (pH=9.177)) were used. The calculation of $[H^+]$ from the measured pH values was performed with the use of the method proposed by Irving *et al.* [20] by titrating a 0.01 M HCl solution ($I=0.15$ M NaCl) with a standardized NaOH solution (from the data collected in the pH range of 1.75-2.2). The K_{MLOH} was calculating with equation (1).

$$K_{MLOH} = \frac{[ML]}{[MLOH][H^+]} \quad (1)$$

The differences between the measured and calculated pH values were used to obtain the $[H^+]$ concentrations from the pH-data obtained in the titrations. The ion product of water was determined from the same experiment in the pH range 11.2-11.9.

The concentration of the ligand stock solution was determined by pH-potentiometric titration from the titration data obtained in the presence and absence of large Mn^{2+} excess. In the pH-

potentiometric titrations of the ligand 186 data pairs were recorded in the pH range of 2.77-11.85, while the sample containing the Mn^{2+} ion (one equivalent) was titrated in the pH range of 3.46-11.86 when 126 data pairs were collected and fitted. The protonation and stability constants were calculated from the titration data with the PSEQUAD program [21].

2.6. Spectroscopic experiments

Absorption spectra were recorded in diluted solution *ca.* 10^{-2} or 10^{-3} mM in CH_2Cl_2 (spectrophotometric grade) on a JASCO V-650 spectrophotometer. Emission and excitation spectra were recorded using a Horiba-Jobin-Yvon Fluorolog-3 fluorimeter. The steady state luminescence was excited by unpolarized light from a 450 W xenon continuous wave lamp and detected at an angle of 90° for measurements of dilute solutions (10 mm quartz cuvette) either by a Hamamatsu R928 or Peltier cooled R2658 photomultiplier tube. Luminescence quantum yield Φ were measured in diluted solutions with an absorbance lower than 0.1 and were determined using coumarin or quinine as references ($\Phi_r = 0.45$ and 0.54 respectively).

2.7. Electrochemistry

The electrochemical studies were performed in a glovebox (Jacomex) ($\text{O}_2 < 1$ ppm, $\text{H}_2\text{O} < 1$ ppm) with a home-designed 3-electrode cell (WE: glassy carbon, RE: Ag/AgCl/NaCl (3 M), CE: graphite rod). The potential of the cell was controlled by using an AUTOLAB PGSTAT 302 (Ecochemie) potentiostat monitored by using a computer. The glassy carbon electrode was carefully polished before each voltammetry experiment with a 1 μm alumina aqueous suspension and ultrasonically rinsed in water and then with acetone. Exhaustive electrolysis was performed with a graphite rod working electrode. The ultrapure (18 $\text{M}\Omega$) deoxygenated water was used as received and kept under argon in the glovebox after degassing. Sodium perchlorate (Sigma-Aldrich, 99.99%) was used as a background

electrolyte in 0.1 M concentration without purification.

1. Results and Discussion

1.1. Synthesis of the ligands and complexes

The synthesis of 1-{2-carboxy-4-[4-ethynyl-*N,N*-bis(3,6,9-trioxodecyl)aniline]}pyridin-2-ylmethyl-4,7-bis(pyridin-2-ylmethyl)-1,4,7-triazacyclononane **HL1** (Scheme 1) started from the previously described 4,7-bis(pyridin-2-ylmethyl)-1,4,7-triazacyclononane **no2py** compound [13], which reacted in dry acetonitrile with 1 equivalent of the mesylated antenna **a** (Methyl 4-[4-ethynyl-*N,N*-bis(3,6,9-trioxodecyl)aniline]-6-[(methylsulfonyloxy)methyl]-2-picolinate) to give intermediate **1**, isolated with a 51% yield after purification by column chromatography. Deprotection of the methyl ester group was then readily achieved in a KOH/THF medium, the targeted product **HL1** being eventually purified by dialysis to eliminate the remaining salts. The preparation of 1-{2-carboxy-4-[4-ethynyl-*N,N*-bis(3,6,9-trioxodecyl)aniline]}pyridin-2-ylmethyl-1,4,7-triazacyclononane **HL2** involved an alternative approach to the one used for the synthesis of the parent **Hno1pa** ligand [14], mostly to avoid the use of strongly acidic conditions hardly incompatible with the structure of fragment **a**. The simultaneous

N-protection of two secondary amines available on the tacn skeleton was achieved with 1 equivalent of benzaldehyde at room temperature in anhydrous EtOH. The resulting aminal product **2** was obtained without purification as a white solid with 97% yield. This protected macrocycle then reacted with 1 equivalent of the mesylated antenna **a**. It should be mentioned that the purification of the crude product on activated alumina led to the cleavage of the aminal protection to produce the desired mono-*N*-functionalized tacn 1-{4-[4-ethynyl-*N,N*-bis(3,6,9-trioxodecyl)aniline]-2-methoxycarbonyl}pyridin-2-ylmethyl-1,4,7-

triazacyclononane **3** with 62% yield (calculated for two steps; 1- *N*-alkylation; 2- deprotection of the aminal-bridged phenyl group). Finally, hydrolysis of the methyl ester function was carried out in 1 M KOH/THF at 55°C for 3 h. The targeted ligand **HL2** was obtained as a yellow oil with a 95% yield after purification, performed *via* semi-preparative HPLC. All final ligands and reaction intermediates have been fully characterized by standard techniques (see Supporting Information for details, Figure S7 to S15).

Finally, the targeted $[\text{Cu}(\mathbf{L1})]^+$ and $[\text{Zn}(\mathbf{L1})]^+$ complexes have been obtained after heating at 60°C for 24 h in a neutral aqueous mixture of **HL1** with 1 molar equivalents of copper and zinc perchlorate, respectively. After evaporation of the solvent followed by dialysis, both complexes have been isolated as yellow oils with 94 and 90% yield, respectively. The HPLC and HR-MS data collected of these complexes are provided in the ESI section (Supporting Information for details, Figures S16 to S19). The complexation of **HL2** with manganese (II) was also attempted following a similar procedure and the desired complex was isolated in 60% yield. All our attempts to obtain consistent MS data failed, but experimental evidences supporting the formation of manganese complex in solution have nevertheless been provided by potentiometric titration and relaxation experiments, allowing to isolate the monometallic complex $[\text{Mn}(\mathbf{L2})]^+$. The analytical HPLC data are provided in Supporting Information (Figure S20).

[Scheme 1 here]

1.2. Copper-64 radiolabeling

Radiolabeling studies have been conducted on freshly prepared ammonium acetate buffer (pH 5.5) solutions containing **HL1** and $^{64}\text{CuCl}_2$ (58 μM). After stirring the mixture for 15 min at

100°C, the radiochemical conversion was monitored by radio-TLC. The resulting thin layer radiochromatograms showing the measured radioactive emission on a storage phosphor screen after 15 min, is depicted in Figure 2. In contrast to the quantitative radiolabeling observed with the parent **Hno2py1pa** ligand, we found that the labeled complex $[^{64}\text{Cu}(\mathbf{L1})]^+$ is formed with a rather modest yield of about 40%. This result supports the conclusion that the picolinate-based ligand is not best suited to chelate ^{64}Cu and that further modifications of the ligand will be needed to enhance the complexation.

[Figure 2 here]

1.3. Potentiometric and relaxometric measurements

Potentiometric experiments were performed in order to gain insights about the complexation properties of **HL2** (see titration curves in Supporting Information, Figure S21). We initially assumed that the presence of the antenna should not affect the complexation ability of the ligand and that similar binding constants should be obtained with **HL2** and **Hno1pa**. The acid-base and the complex formation constants were firstly determined in aqueous media and the data obtained with **HL2** were systematically compared to the values collected with the parent **Hno1pa** ligand [14]. All acid-base and metal complexation studies were performed by pH-potentiometric titrations in aqueous solution at 25.0 ± 0.1 °C and 0.15 ± 0.01 M NaCl. The stepwise formation constants K_i^{H} calculated for **HL2** are collected in Table 1 along with those determined for **Hno1pa**, while overall ($\log \beta_i^{\text{H}}$) species distribution diagrams calculated are shown in Supporting Information (respectively Table S1 and Figure S22). With an overall protonation constant ($\log \beta_3$) of 22.12, **HL2** possesses nearly the same total basicity as **Hno1pa** ($\log \beta_3 = 21.12$) [14]. Both ligands display three protonation constants and the first one ($K_1 \approx 11.4$) can be assigned to the protonation of one of the secondary amines of the

macrocycle. The second protonation ($\log K_2 \approx 7.46$) occurs also at the secondary amine nitrogen of the tacn skeleton. Finally, the third protonation constant ($\log K_3 \approx 3.25$), attributed to the protonation of the carboxylic function of the picolate arm, was found to be significantly larger than the one determined for **Hno1pa**.

[Table 1 here]

The complexation of Mn(II) was evaluated from pH-potentiometric titration experiments carried out in a sample containing a 1:1 metal-to-ligand ratio. Since complexation was not quantitative at acidic pH, the stability constants associated to the formation of $[\text{MnL2}]^+$ could be assessed in the absence of competitor. The calculated equilibrium constants are reported in Table 2 while the speciation distribution curves calculated with the use of these data are shown in Figure 2.

[Table 2 here]

The formation constant determined for $[\text{MnL2}]^+$ complex is slightly larger ($\Delta \log K_{\text{MnL}} = 0.28$) than that obtained in the same conditions with **Hno1pa**. A second formation constant of 11.62 was measured for the hydroxo complex $[\text{MnL2}(\text{OH})]$. A detailed analysis of the species distribution diagram indicates that the complexation of **HL2** starts at $\text{pH} > 4$ and becomes quantitative near to the physiological pH ($\text{pH}=7.4$) up to $\text{pH}=10$.

For a better comparison of the thermodynamic stability constant of the Mn(II) complex formed with **HL2** and values obtained in the literature for different Mn(II)-based contrast agents, the pM values ($\text{pM} = -\log [\text{M}^{n+}]$) that take into account the different basicity of the

ligands were also calculated (Table 2) using the conditions described by Tóth *É et al.* for Mn(II) complexes ($[\mathbf{L2}] = [\text{Mn(II)}] = 10 \mu\text{M}$ at pH 7.4) [26]. The pMn value of 7.21 obtained for **HL2** is nearly identical to the one obtained for the complex of **Hno1pa** ($\Delta\text{pMn} = 0.13$) but it is still slightly lower than the value calculated for $[\text{Mn}(\mathbf{PyC3a})]^-$ described by Caravan *et al.* [15] and for the complex formed with the tri-*N*-acetate tacn ligand **H3nota** [24]. To conclude, while our first attempts to confirm the formation of the $[\text{Mn}(\mathbf{L2})]^+$ complex were not successful, we were able to prove the formation of this complex by pH-potentiometry, relaxometry and HPLC techniques. The introduction of an extended π -conjugated system at the *para* position of the picolate arm does not impact the coordination properties of the ligand and it also leads to a thermodynamically stable Mn(II) complex possessing comparable stability to other tacn based chelates cited before.

The relaxation properties of $[\text{Mn}(\mathbf{L2})]^+$ have then been measured by low field NMR relaxometry and then compared to data measured in the same conditions with the free ligand **HL2**, with particular focus on the proton relaxivity, r_{1p} , which refers to the relaxation enhancement of water protons promoted by a 1 mM concentration of the Mn^{2+} cation. The r_{1p} values obtained for the Mn^{2+} complex $[\text{Mn}(\mathbf{L2})]^+$ was recorded simultaneously with potentiometric titration data collected during a titration experiment. The relative relaxivity data and the molar fraction obtained by potentiometric measurements are plotted together as a function of pH on the graph depicted in Figure 3.

[Figure 3 here]

The r_{1p} value obtained for the $[\text{Mn}(\mathbf{L2})]^+$ complex at 60 MHz, 298 K and pH = 8.15 is $4.80 \text{ mM}^{-1} \cdot \text{s}^{-1}$. This value is in agreement with the presence of one water molecule in the inner sphere of the Mn^{2+} center, which was already described for the parent complex formed with

Hno1pa [14]. The relaxivity of $[\text{Mn}(\mathbf{L2})]^+$ is found to be much larger than those reported in literature for other Mn^{2+} contrast agents, including several ones concerning the FDA-approved Gd^{3+} -based contrast agents (for example Dotarem[®] in water $r_{1p} = 3.4 \text{ mM}^{-1} \cdot \text{s}^{-1}$ at 20 MHz

(313 K) and $2.9 \text{ mM}^{-1} \cdot \text{s}^{-1}$ at 60 MHz (310 K)) [27]. Interestingly, the complex $[\text{Mn}(\mathbf{L2})]^+$ also possesses a r_{2p} value of $8.72 \text{ mM}^{-1} \cdot \text{s}^{-1}$ which was unfortunately not determined for the parent Mn^{2+} complex ($[\text{Mn}(\mathbf{no1pa})]^+$).

It can be reasonably assumed that the significant increase in the r_{1p} and r_{2p} values is related to the large increase in mass resulting from the introduction of both the π -conjugated antenna and of the hydrosolubilizing PEG groups attached to the tacn platform. This interesting result opens the way for the use of such complex as a T_1 or T_2 shortening MRI relaxation agent.

1.4. Photophysical and electrochemical properties.

The photophysical properties (absorption, emission, quantum yield) of the complexes were investigated in organic solvent (CH_2Cl_2). Most of these data are collected in Table 3, while the absorption/emission spectra are given in Supporting Information section (Figures S23-S26). The absorption and emission spectra of all the investigated compounds show a broad band in the visible range which can be assigned to an Intra-Ligand Charge Transfer transition (ILCT) from the N-donor atom to the picolinic acceptor unit. As expected, the $[\text{M}(\mathbf{L1})]^+$ ($\text{M} = \text{Cu}, \text{Zn}$) complexes present very similar spectra due to their comparable Lewis acidity. Nevertheless, the comparison of their luminescent quantum yield shows a modest 5% yield in the case of zinc, similar to what is observed for the free ligand (Figure S22 in Supporting Information) that is strongly reduced to less than 1% in the case of copper. This quenching is not observed in the case of $[\text{Mn}(\mathbf{L2})]^+$, featuring a slightly blue shifted emission with a quantum yield efficiency of about 8%.

[Table 3 here]

The quenching monitored upon copper (II) complexation is a common phenomenon which has been widely described in the literature [28-30]. It is generally explained by a photo-induced electron transfer mechanism whose thermodynamic feasibility can be readily assessed from the following Rehm-Weller equation (2) [31].

$$\Delta G = E_{ox}(D) - E_{red}(A) - E^* + C \quad (2)$$

In this equation $E_{ox}(D)$ corresponds to the oxidation potential of the ILCT transition antenna unit and $E_{red}(A)$ to the reduction potential of the Cu(II) complex while E^* refers to the excited-state energy and C represents a Coulombic term (neglected in this experiment).

The $E_{red}(A)$ and $E_{ox}(D)$ values have been readily obtained upon carrying electrochemical measurements. The cyclic voltammogram (CV) recorded for $[\text{Cu}(\mathbf{L1})]^+$ in aqueous medium (0.1 M LiClO_4) by using a carbon working electrode is shown in Figure 4. The curve displays an irreversible oxidation process centered at $E_{peak} = +0.91$ V attributed to the oxidation of the donor part of the fluorescent antenna ($E_{ox}(D)$), together with a quasi-reversible copper-centered reduction wave at $E_{1/2} = -0.54$ V ($\Delta E_p = 120$ mV at 100 mV/s) which was approximated to the formal potential $E^{\circ'}([\text{Cu}^{\text{II}}(\mathbf{L1})]^+ / [\text{Cu}^{\text{I}}(\mathbf{L1})]) = E_{red}(A)$. Finally, the excited-state energy for this complex was estimated by the zero-phonon energy, E_{00} corresponding to the intersection of the absorption and emission curves and a value of 2.72 eV was found in CH_2Cl_2 (Figure S23 in Supporting Information). According to the Rehm-Weller equation, the resulting ΔG value was found to be roughly -1.27 eV. This

negative value allows us to predict that the electron transfer process is favorable in this complex and is a reasonable explanation for the observed luminescence quenching.

[Figure 4 here]

The apparent reversibility of the reduction wave observed at $E_{1/2} = -0.54$ V suggests that the electrogenerated copper(I) complex $[\text{Cu}^{\text{I}}(\text{L1})]$ is stable at the CV time scale and that there is no chemical step (isomerization, degradation etc.) coupled to the electron transfer under these experimental conditions. A similar behavior was observed in DMF electrolyte (Figure 5B). In-situ spectro-electrochemical (SEC) analyses have thus been carried out in the latter conditions to obtain further insights into the nature and stability of the $[\text{Cu}^{\text{I}}(\text{L1})]$ species.

SEC measurements carried out in the UV-Vis range using an optically transparent thin-layer electrochemical cell showed that the one electron reduction of the $[\text{Cu}^{\text{II}}(\text{L1})]^+$ leads to a gradual disappearance of the signal centered at $\lambda_{\text{max}} = 397$ nm at the expense of a new absorption band growing at $\lambda_{\text{max}} = 377$ nm (Figure 5A). These changes were found to proceed through a well-defined isobestic point at 385 nm only during the first stage of the reduction. Keeping the potential of the working electrode at $E_{\text{app}} = -1.1$ V for a prolonged time indeed led to a progressive increase of the intensity at 377 nm (dashed line in Figure 5A). The whole process was however found to be reversible as the intensity of the initial signal attributed to $[\text{Cu}^{\text{II}}(\text{L1})]^+$ could be recovered upon scanning the electrode potential back to $E_{\text{app}} = 0$ V.

Overall these experiments reveal that the $[\text{Cu}^{\text{I}}(\text{L1})]$ seems stable at the electrolysis time scale and that its absorption band is hypsochemically shifted by about 20 nm compared to that of the copper(II) complex in agreement with the reduced Lewis acidity of Cu(I) compared to Cu(II).

[Figure 5 here]

1.5. Confocal Microscopy

Finally, preliminary cell imaging experiments have been undertaken using the most luminescent $[\text{Zn}(\mathbf{L1})]^+$ on MDA-MB 468 cell-line. In our hand this complex was not able to stain spontaneously living cells by passive internalisation processes as already observed for other cationic complexes [16,17,32]. Consequently, PFA-fixed cells have been used to illustrate the proof-of-concept of fluorescence bioimaging of this complex. (Figure 5) $10\ \mu\text{M}$ of $[\text{Zn}(\mathbf{L1})]^+$ were added to the culture medium and incubated for 1h with fixed cells. The images were acquired under 385 nm excitation and a broadband detection between 500 to 600 nm. The slight green luminescence in the cells (Figure 6) indicates that the cationic complex is able to accumulate in fixed cells, more precisely in the perinuclear cytoplasmic area and in the nucleoli as observed for lanthanide species featuring similar π -conjugated antennas [16-17].

[Figure 6 here]

2. Conclusion

In this article, we describe the results of our first attempt to implement a luminescence modality on existing scaffold suitable for ^{64}Cu -PET or Mn(II)-based MRI applications by functionalizing the picolinate pendant arm with a donor π -conjugated chromophore antenna in order to combine two imaging modalities in a single candidate. The cationic complexes $[\text{M}(\mathbf{L1})]^+$ ($\text{M} = \text{Cu}, \text{Zn}$) and $[\text{M}(\mathbf{L2})]^+$ ($\text{M} = \text{Mn}$) have been prepared and fully characterized.

The results we obtained are contrasted: in the case of copper, the picolinate functionalization induced a modification of the chelation properties leading to an uncompleted radiolabeling and the emission properties of the antenna have been quenched by a photo-induced electron transfer process; however, results obtained with Zn^{2+} clearly show the viability of the concept since cells images have been obtained. In the case of manganese, the results are more promising than it was found for the parent complex formerly since the $[\text{Mn}(\mathbf{L2})]^+$ complex presents improved relaxation properties better than that of the $[\text{Gd}(\text{DOTA})]^-$ (the active ingredient of Dotarem® which is the most trusted contrast agent on the market) accompanied with acceptable luminescence properties. This complex presents a double-imaging modality potential (MRI and optical imaging) and is the first step towards the design of a real bimodal probe.

3. Conflict of interest

The authors declare no conflict of interest.

4. Acknowledgements

The authors acknowledge support of the Ministère de l'Enseignement Supérieur et de la Recherche, the Centre National de la Recherche Scientifique, the Institut National de la Santé et de la Recherche Médicale and the Agence Nationale de la Recherche (SADAM ANR-16-CE07-0015-02). R.T. thanks the "Service Commun de RMN" of the University of Brest. Gy.T. acknowledges financial support arriving from the Hungarian National Research, Development and Innovation Office (NKFIH K-120224 project), János Bolyai Research Scholarship of the Hungarian Academy of Sciences and European Regional Development Fund under the project GINOP-2.3.2-15-2016-00008.

References

- [1] E.W. Price, C. Orvig, *Chem. Soc. Rev.* 43 (2013) 260–290.
- [2] E. Boros, A.B. Packard, *Chem. Rev.* 119, 2 (2019) 870-901
- [3] L.E. Jennings, N.J. Long, *Chem. Commun.* (2009) 3511–3524.
- [4] A. Louie, *Chem. Rev.* 110 (2010) 3146–3195.
- [5] E. Ranyuk, R. Lebel, Y. Bérubé-Lauzière, K. Klarskov, R. Lecomte, J.E. van Lier, B. Guérin, *Bioconjugate Chem.* 24 (2013) 1624–1633.
- [6] T. Joshi, M. Kubeil, A. Nsubuga, G. Singh, G. Gasser, H. Stephan, *ChemPlusChem* 83 (2018) 554–564.
- [7] T.J. Wadas, E.H. Wong, G.R. Weisman, C.J. Anderson, *Chem. Rev.* 110 (2010) 2858–2902.
- [8] J. Wahsner, E.M. Gale, A. Rodríguez-Rodríguez, P. Caravan, *Chem. Rev.* 119 (2019), 957-1057.
- [9] A.J. Amoroso, S.J.A. Pope, *Chem. Soc. Rev.* 44, 14 (2015) 4723–4742.
- [10] R.M. Izatt, K. Pawlak, J.S. Bradshaw, R.L. Bruening, *Chem. Rev.* 91, 8 (1991) 1721–2085.
- [11] M. Le Fur, M. Beyler, N. Le Poul, L.M.P. Lima, Y. Le Mest, R. Delgado, C. Platas-Iglesias, V. Patinec, R. Tripier, *Dalton Trans.* 45, 17 (2016) 7406–7420.
- [12] A. Nonat, D. Imbert, J. Pécaut, M. Giraud, M. Mazzanti, *Inorg. Chem.* 48, 9 (2009) 4207–4218.
- [13] M. Roger, L.M.P. Lima, M. Frindel, C. Platas-Iglesias, J.-F. Gestin, R. Delgado, V. Patinec, R. Tripier, *Inorg. Chem.* 52 (2013) 5246–5259.
- [14] E. Molnár, N. Camus, V. Patinec, G.A. Rolla, M. Botta, G. Tircsó, F.K. Kálmán, T. Fodor, R. Tripier, C. Platas-Iglesias, *Inorg. Chem.* 53 (2014) 5136–5149.

- [15] E.M. Gale, I.P. Atanasova, F. Blasi, I. Ay, P. Caravan, *J. Am. Chem. Soc.* 137 (2015) 15548–15557.
- [16] A.T. Bui, M. Beyler, Y.-Y. Liao, A. Grichine, A. Duperray, J.-C. Mulatier, B. Le Guennic, C. Andraud, O. Maury, R. Tripier, *Inorg. Chem.* 55 (2016) 7020–7025.
- [17] A.T. Bui, M. Beyler, A. Grichine, A. Duperray, J.-C. Mulatier, Y. Guyot, C. Andraud, R. Tripier, S. Brasselet, O. Maury, *Chem. Commun.* 53 (2017) 6005–6008.
- [18] A. D'Aléo, A. Picot, A. Beeby, J.A. Gareth Williams, B. Le Guennic, C. Andraud, O. Maury, *Inorg. Chem.* 47 (2008) 10258–10268.
- [19] A. D'Aléo, A. Picot, P.L. Baldeck, C. Andraud, O. Maury, *Inorg. Chem.* 47 (2008) 10269–10279.
- [20] H.M. Irving, M.G. Miles, L.D. Pettit, *Anal. Chim. Acta*, 38 (1967) 475–488.
- [21] L. Zekany, I. Nagypal, in *Comput. Methods Determ. Form. Constants* (Ed.: D.J. Leggett), Springer US, Boston, MA (1985) pp. 291–353.
- [22] A.A. Belal, L.H. Abdel-Rahman, A.H. Amrallah, *J. Chem. Eng. Data* 42 (1997) 1075–1077.
- [23] B. Drahoš, V. Kubíček, C.S. Bonnet, P. Hermann, I. Lukeš, E. Tóth, *Dalton Trans.* 40 (2011) 40, 1945-1951.
- [24] S. Cortes, E. Brucher, C.F.G.C. Geraldes, A.D. Sherry, *Inorg. Chem.*, 29 (1990) 5-9.
- [25] A. Sá, C.S. Bonnet, C.F. Geraldes, É. Tóth, P.M. Ferreira, J.P. André, *Dalton Trans.* 2013, 42(13), 4522-4532.
- [26] C. Paul-Roth, K.N. Raymond, *Inorg. Chem.* 34 (1995) 1408–1412.
- [27] M. Rohrer, H. Bauer, J. Mintorovitch, M. Requardt, H.-J. Weinmann, *Invest. Radiol.* 40 (2005) 715-724.
- [28] Z. Liu, Z. Yang, T. Li, B. Wang, Y. Li, D. Qin, M. Wang, M. Yan, *Dalton Trans.* 40 (2011) 9370–9373.

- [29] L. Sun, D. Hao, W. Shen, Z. Qian, C. Zhu, *Microchim. Acta* 177 (2012) 357–364.
- [30] N. Chopin, M. Médebielle, O. Maury, G. Novitchi, G. Pilet, *Eur. J. Inorg. Chem.* 36 (2014) 6185–6195.
- [31] D. Rehm, A. Weller, *Isr. J. Chem.* 8 (1970) 259–271.
- [32] J.W. Walton, A. Bourdolle, S.J. Butler, M. Soulie, M. Delbianco, B.K. McMahon, R. Pal, H. Puschmann, J.M. Zwier, L. Lamarque, O. Maury, C. Andraud, D. Parker, *Chem. Commun.* 49 (2013) 1600–1602.

Journal Pre-proof

Tables

Table 1. Stepwise ($\log K_i^H$) protonation constants of **HL2** in aqueous solution at 25.0 ± 0.1 °C and 0.15 ± 0.01 M NaCl.

Equilibrium reaction	HL2	Hno1pa [14]
	log <i>K</i>	
$L + H^+ \rightleftharpoons HL$	11.41(1)	11.33
$HL + H^+ \rightleftharpoons H_2L$	7.46(3)	7.30
$H_2L + H^+ \rightleftharpoons H_3L$	3.25(3)	2.49

Table 2. Stability constants ($\log K$) for the metal complexes of the ligands in aqueous solution at 25.0 ± 0.1 °C and 0.15 ± 0.01 M NaCl.

	log K_{MnL}	log K_{MnL}^{OH}	pMn	Reference
H₃PyC3a	14.14	-	8.17	15
Tacn	8.33	-	6.37	22
H₃nota	14.9	-	7.76 ; 7.94	23; 24
NODAHep	10.98	-	5.73	25
NODAHA ^a	10.15	9.65	5.76	25
NODABA	9.9	-	5.60	25
Hno1pa	10.28	11.94	7.08	14
HL2	10.56(4)	11.62(5)	7.21	This work

^a the formation of a protonated complex was also observed for the given system ($\log K_{MnL}^H = 4.95$)

Table 3. Photophysical data measured in CH_2Cl_2 for studied ligands and metal complexes

Compound	Solvent	λ_{abs} (nm)	λ_{em} (nm)	Φ^a (%)
$[Cu(L1)]^+$	CH_2Cl_2	410	507	< 1
$[Zn(L1)]^+$	CH_2Cl_2	407	570	5
$[Mn(L2)]^+$	CH_2Cl_2	315	464	8

^a Coumarin 153 in MeOH ($\Phi = 45\%$) for **L1** species and Quinine sulfate in H_2SO_4 1N ($\Phi = 54\%$) for **L2** species as standards

Figures and Schemes Captions

Figure 1. Tacn-based ligands investigated as part of the present article.

Figure 2. Thin layer radiochromatograms of $^{64}\text{Cu}(\text{CO}_2\text{Me})_2$ (A) and $[^{64}\text{Cu}(\text{L1})]^+$ (B) and % of ^{64}Cu emission; 58 μM ligand and 15 min incubation time in ammonium acetate buffer at 100°C.

Figure 3. Species distribution diagram of the complex $[\text{Mn}(\text{L2})]^+$ calculated in the pH range of 3 to 11 (calculated by using 1 mM of Mn^{2+} and ligand; plain lines) and the plots of the $1/T_1$ (●) and $1/T_2$ (s^{-1}) (▲) values evaluated at 60 MHz and 0.15 M NaCl at 298 K (dashed lines).

Figure 4. Cyclic voltammogram (0.1 $\text{V}\cdot\text{s}^{-1}$, GC carbon WE $\varnothing = 3\text{mm}$, H_2O , pH 7, 0.1 M LiClO_4) and absorption/emission spectra of $[\text{Cu}(\text{L1})]^+$ (CH_2Cl_2).

Figure 5. A) UV–Vis abs. spectra recorded during the one-electron reduction of $[\text{Cu}^{\text{II}}(\text{L1})]^+$ in DMF (0.1 M TBAP). The reduction was carried out in an optically transparent thin-layer electrochemical cell ($l = 1\text{mm}$) using a platinum gauze working electrode whose potential was linearly scanned (10 mV/s) between 0 and -1.1 V. The spectrum recorded at the end of the reduction is shown as a dashed line; B) Voltammetric curves of a DMF (TBAP 0.1 M) solution of $[\text{Cu}(\text{L1})]^+$ recorded at a stationary carbon working electrode ($\varnothing = 3\text{ mm}$, E vs Ag^+/Ag (10^{-2} M), $\nu = 0.1\text{ V}\cdot\text{s}^{-1}$).

Figure 6. Confocal microscopy images of MDA-MB cells before (A) and after 1h of incubation with the $[\text{Zn}(\text{L1})]^+$ at 10 μM (B)

Scheme 1. Synthesis of the ligands and complexes studied in this work. i) adapted from ref 13; ii) benzaldehyde, molecular sieves, EtOH, rt 4h; iii) antenna **a**, K₂CO₃, CH₃CN, rt, 72h; iv) 1M KOH, THF, 55°C, 12h. v) M^{II}(ClO₄)₂·6H₂O (M^{II} = Cu²⁺ / Zn²⁺), H₂O, pH 6.6, 60°C, 24h; vi) MnCl₂·4H₂O, H₂O, neutral pH, 60°C, 24h.

Journal Pre-proof

Figures and Schemes

Figure 1.

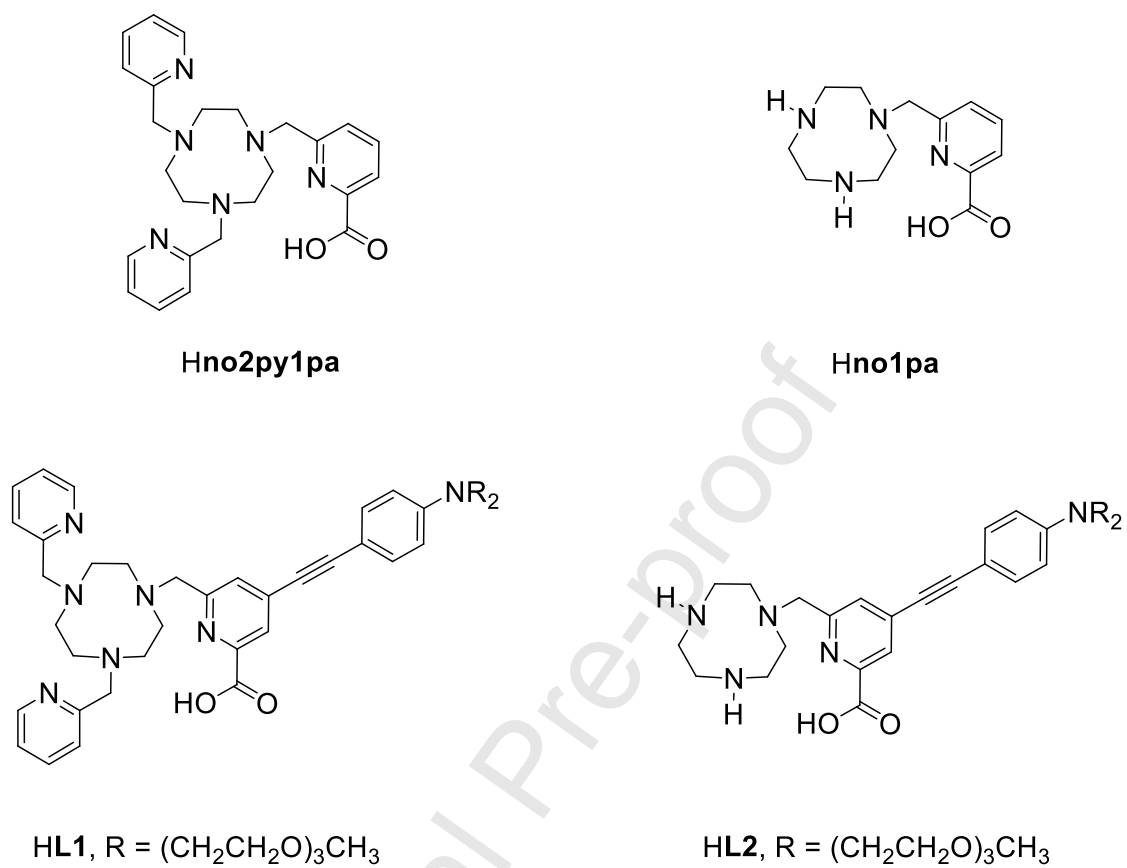


Figure 2.

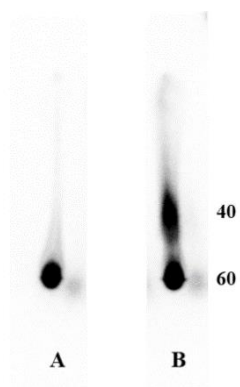


Figure 3.

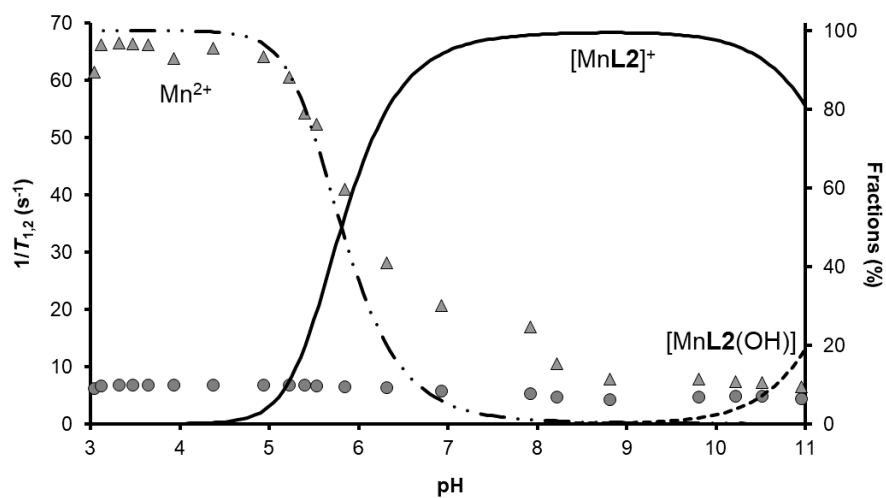


Figure 4.

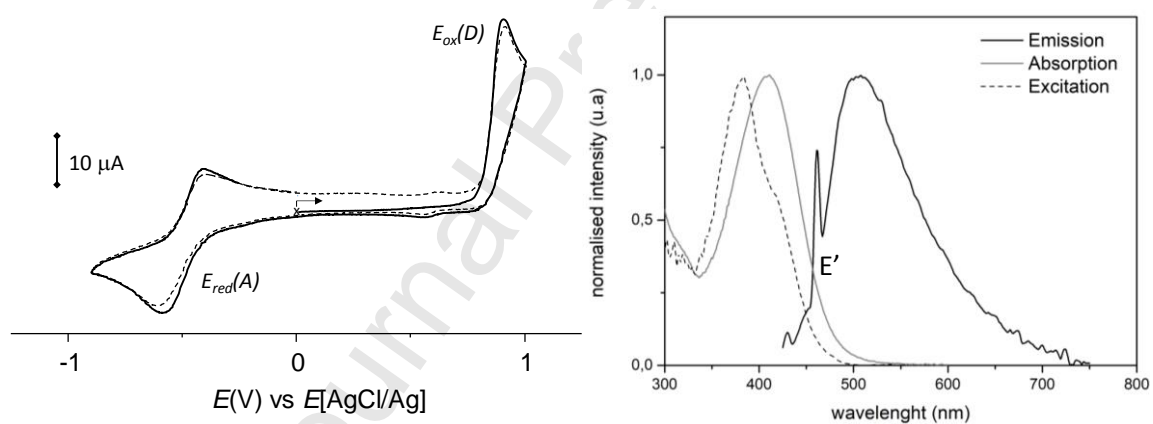


Figure 5.

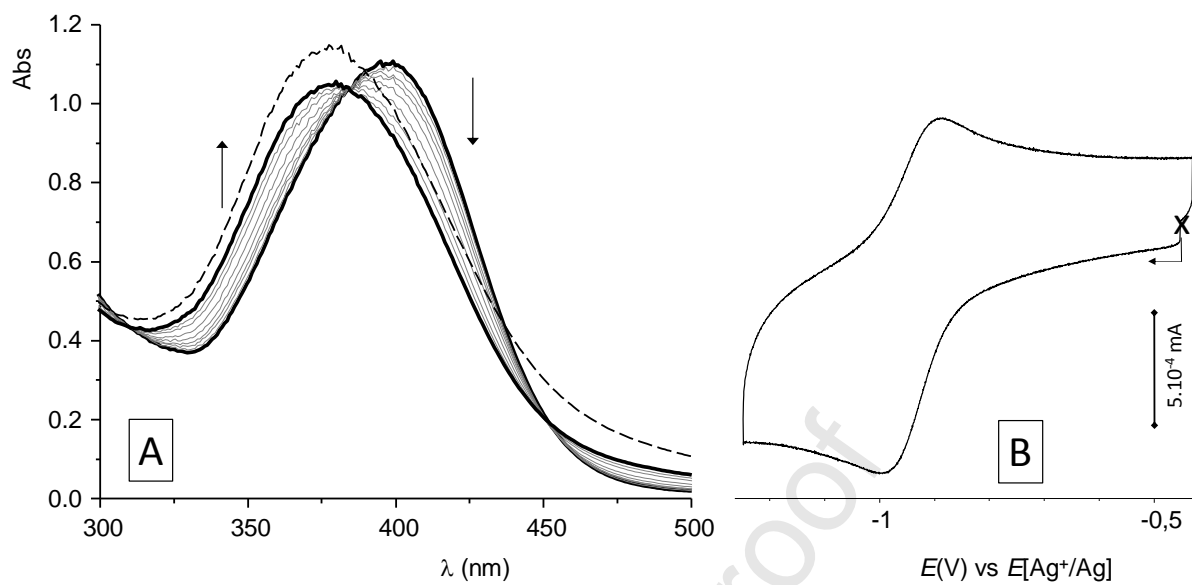
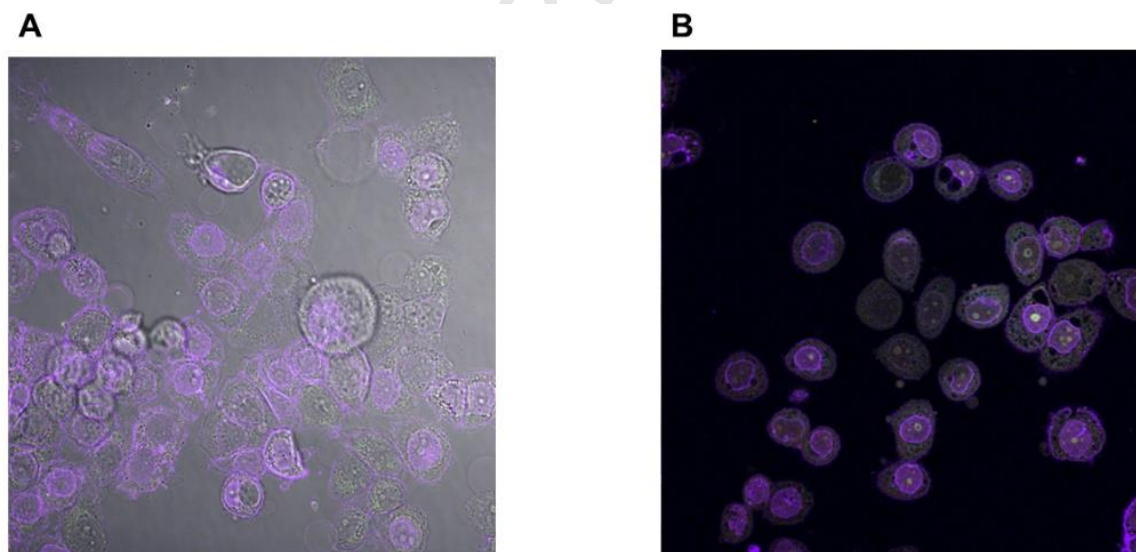
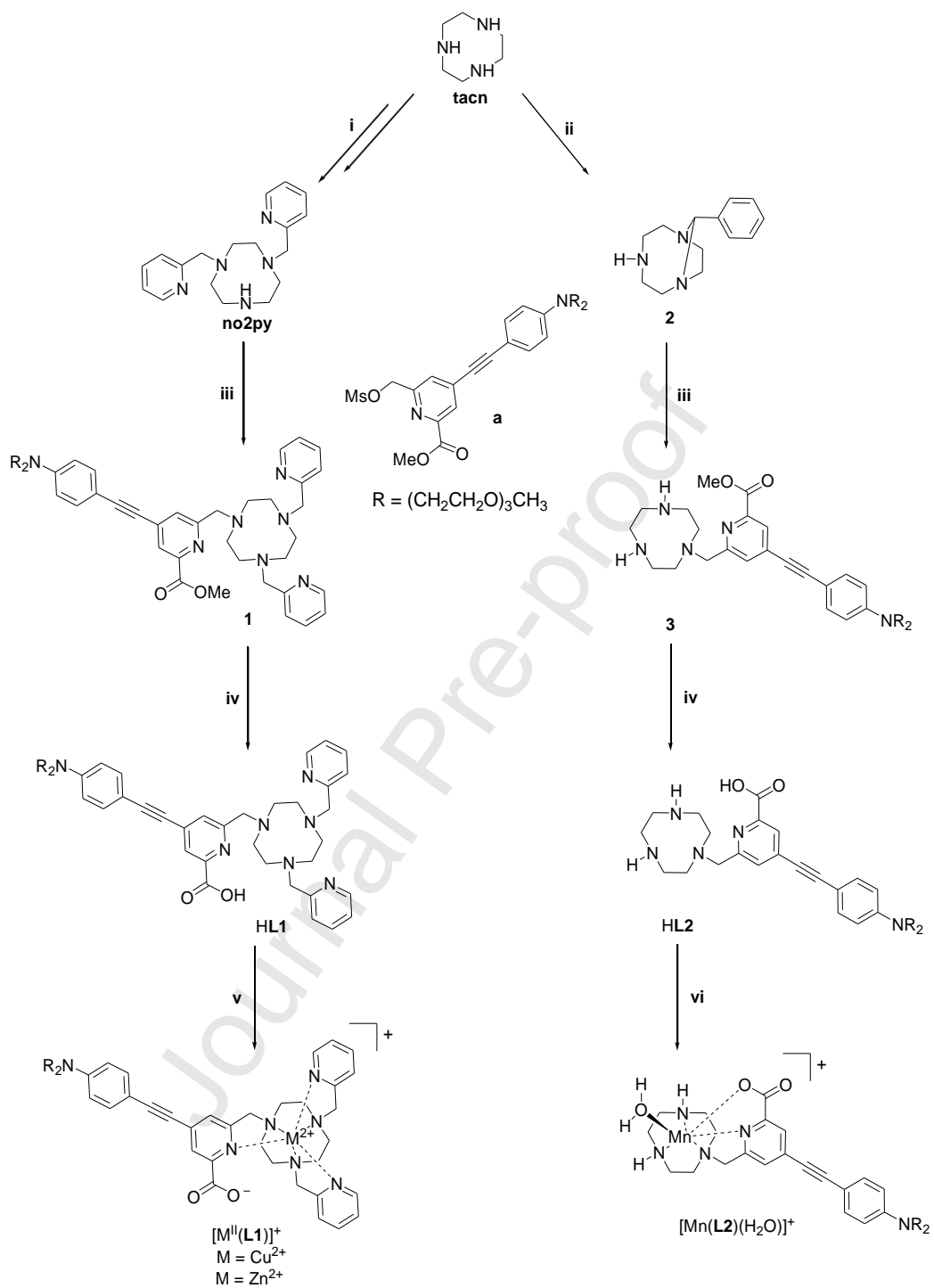


Figure 6.



Scheme 1.



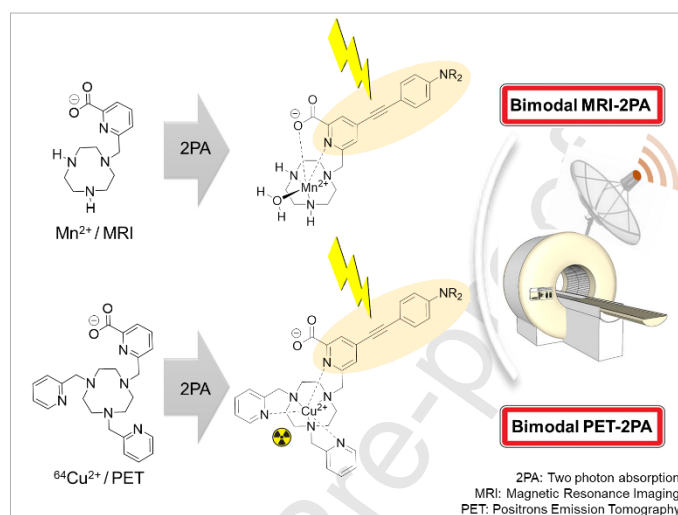
Declaration of interests

The authors declare that they have no known competing financial interests or personal relationships that could have appeared to influence the work reported in this paper.

The authors declare the following financial interests/personal relationships which may be considered as potential competing interests:

Picolinate-Appended Tacn Complexes for Bimodal Imaging: radiolabeling, relaxivity, photophysical and electrochemical studies

TOC graphic



1,4,7-triazacyclononane (tacn)-based Mn^{2+} or Cu^{2+} chelates bearing picolinate-based π -conjugated antenna derived from previously described scaffold suitable for ^{64}Cu -Positrons Emission Tomography or Mn-Magnetic Resonance Imaging applications are investigated to evaluate their relevance as bimodal probes.

Picolinate-Appended Tacn Complexes for Bimodal Imaging: radiolabeling, relaxivity, photophysical and electrochemical studies

Highlights

- Luminescence modality introduced on existing scaffolds suitable other modalities
- Emission properties quenched by a photo-induced electron transfer process with Cu^{2+}
- Emission properties and cell images performant with Zn^{2+}
- Mn^{2+} complex has improved relaxation properties together with emission properties
- Identification of a potential Magnetic Resonance Imaging / optical imaging agent